LETTER

doi:10.1038/nature24630

Photonuclear reactions triggered by lightning discharge

Teruaki Enoto[1], Yuuki Wada[2,3], Yoshihiro Furuta[2], Kazuhiro Nakazawa[2,4], Takayuki Yuasa[5], Kazufumi Okuda[2], Kazuo Makishima[6], Mitsuteru Sato[7], Yousuke Sato[8], Toshio Nakano[3], Daigo Umemoto[9] & Harufumi Tsuchiya[10]

Lightning and thunderclouds are natural particle accelerators[1]. Avalanches of relativistic runaway electrons, which develop in electric fields within thunderclouds[2,3], emit bremsstrahlung γ-rays. These γ-rays have been detected by ground-based observatories[4–9], by airborne detectors[10] and as terrestrial γ-ray flashes from space[10–14]. The energy of the γ-rays is sufficiently high that they can trigger atmospheric photonuclear reactions[10,15–19] that produce neutrons and eventually positrons via β^+ decay of the unstable radioactive isotopes, most notably ^{13}N, which is generated via $^{14}\mathrm{N}+\gamma\rightarrow{}^{13}\mathrm{N}+n$, where γ denotes a photon and n a neutron. However, this reaction has hitherto not been observed conclusively, despite increasing observational evidence of neutrons[7,20,21] and positrons[10,22] that are presumably derived from such reactions. Here we report ground-based observations of neutron and positron signals after lightning. During a thunderstorm on 6 February 2017 in Japan, a γ-ray flash with a duration of less than one millisecond was detected at our monitoring sites 0.5–1.7 kilometres away from the lightning. The subsequent γ-ray afterglow subsided quickly, with an exponential decay constant of 40–60 milliseconds, and was followed by prolonged line emission at about 0.511 megaelectronvolts, which lasted for a minute. The observed decay timescale and spectral cutoff at about 10 megaelectronvolts of the γ-ray afterglow are well explained by de-excitation γ-rays from nuclei excited by neutron capture. The centre energy of the prolonged line emission corresponds to electron–positron annihilation, providing conclusive evidence of positrons being produced after the lightning.

With the aim of detecting γ-rays from powerful and low-altitude winter thunderclouds along the coast of the Sea of Japan, we have been operating radiation detectors since 2006[6,22,23] at the Kashiwazaki-Kariwa nuclear power station in Niigata (see Methods section 'GROWTH collaboration'). On 6 February 2017, a pair of lightning discharges occurred at 08:34:06 UTC, 0.5–1.7 km away from our four radiation detectors (labelled 'A' to 'D', see Fig. 1 and Methods section 'Lightning discharges'). All four detectors simultaneously recorded an intense radiation that lasted for about 200 ms (Fig. 1). The radiation-monitoring stations operated by the power plant also recorded this flash (see Fig. 1a and Methods section 'Radiation monitors'). The analogue outputs of the phototube amplifier exhibited strong 'undershoot' (that is, a negative voltage output was detected, which would never happen during normal operation) at the beginning

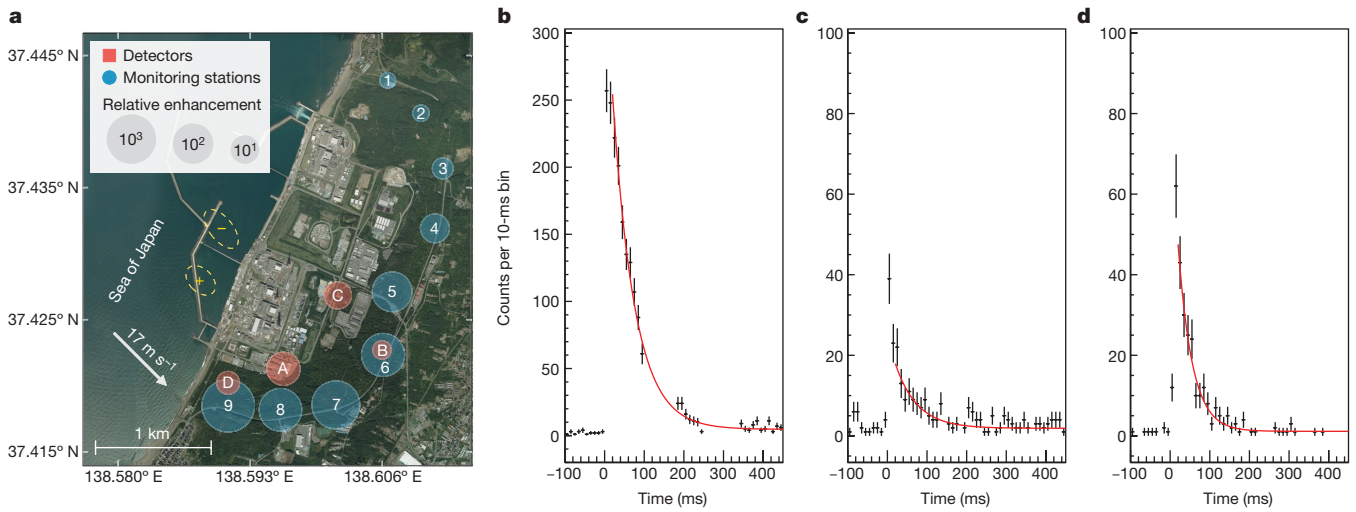

Figure 1 | Lightning discharges and subsecond decaying high-energy radiation. a, Photograph of the observation site. Yellow dashed circles show the positional error of the locations of the negative ('−') and positive ('+') discharges (see Methods section 'Lightning discharges'). Our radiation detectors (red) and the radiation-monitoring stations (blue) are marked by overlaid circles, with the size of the circle indicating the radiation enhancement relative to the environmental background, averaged over the approximately 10 min before and after the lightning. The arrow shows the wind speed and direction. **b**–**d**, Deadtime-corrected 10-ms-binned count-rate histories with $\pm1\sigma$ errors, recorded by detectors A (**b**; >0.35 MeV), B (**c**; >0.35 MeV) and C (**d**; >1.2 MeV). Red lines show the best-fitting model functions of an exponential decay. See Methods section 'Initial flash' for details.

[1]The Hakubi Center for Advanced Research and Department of Astronomy, Kyoto University, Kyoto 606-8302, Japan. [2]Department of Physics, Graduate School of Science, The University of Tokyo, Tokyo 113-0033, Japan. [3]High Energy Astrophysics Laboratory, RIKEN Nishina Center, Saitama 351-0198, Japan. [4]Research Center for the Early Universe, The University of Tokyo, Tokyo 113-0033, Japan. [5]55 Devonshire Road, Singapore 239855, Singapore. [6]MAXI Team, RIKEN, Saitama 351-0198, Japan. [7]Graduate School of Science, Hokkaido University, Sapporo 060-0808, Japan. [8]Department of Applied Energy, Graduate School of Engineering, Nagoya University, Aichi 464-8603, Japan. [9]Advanced Institute for Computational Science, RIKEN, Hyogo 650-0047, Japan. [10]Nuclear Science and Engineering Center, Japan Atomic Energy Agency, Ibaraki 319-1195, Japan.

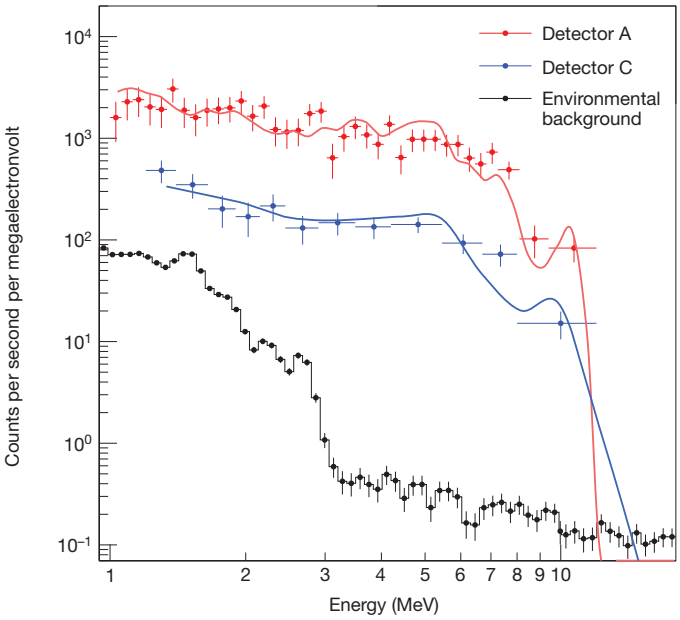

Figure 2 | De-excitation γ-ray spectra of the subsecond afterglow. Background-subtracted radiation spectra of detectors A (red) and C (blue), compared with the simulated de-excitation γ-ray spectra (solid lines). The events are accumulated over 40 ms $< t <$ 100 ms and 20 ms $< t <$ 200 ms, respectively. The background spectrum is also plotted for comparison (black), extracted from -130 s $< t < -10$ s and 90 s $< t <$ 210 s. The read-out deadtime is corrected for detector A; the instrumental response (energy redistribution and energy-dependent effective area) is included for both detectors. The error bars show $\pm 1\sigma$.

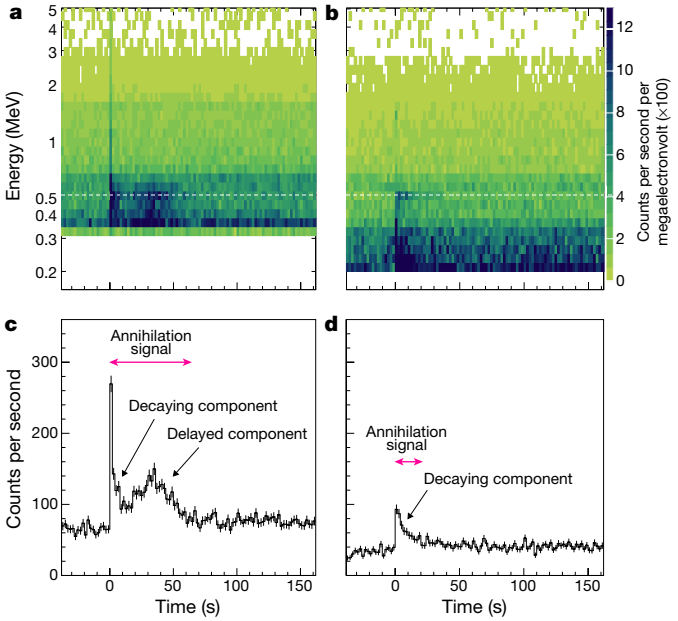

Figure 3 | Count-rate histories of the annihilation signal. a, **b**, Two-dimensional histograms of detected counts, binned in time (1-s binning) and energy, of detectors A (**a**) and D (**b**). The horizontal white dashed line indicates 0.511 MeV. Starting from $t = 0$, the enhancement in the counts is visible in excess of the background signal (for example, that seen for $t < 0$) from cosmic rays (>3 MeV) or environmental radioactive nuclei (<3 MeV). **c**, **d**, 2-s-binned 0.35–0.60-MeV count-rate histories (1σ errors) of detectors A (**c**) and D (**d**). Pink arrows indicate the times from which spectra of annihilation signals (Fig. 4) are accumulated (1.0 s $< t <$ 63 s in **c**; 1.0 s $< t <$ 20 s in **d**).

of the event for roughly 40 ms, 20 ms, 20 ms and 300 ms in detectors A–D, respectively (see Methods section 'Initial flash'). These undershoots are an instrumental response to intensive outputs from the scintillation crystals in our detectors that greatly exceed the nominal dynamic range of the instrument, and were triggered by a very short (less than 1 ms) and strong γ-ray flash that resembled a downward terrestrial γ-ray flash[24]. In the following analyses, we define t as the time from the epoch of the rise of the initial radiation flash.

After the initial surge of signals and after the nominal operation status of the amplifier had been restored (see Methods section 'Initial flash'), all of the detectors recorded subsecond afterglow (Fig. 1b–d). The time profile is fitted satisfactorily by an exponential form with a decay constant of 40–60 ms. The event rates that were recorded with detectors A–C above 3 MeV during the subsecond afterglow are 2–3 orders of magnitude higher than the environmental background. The spectra show a power-law shape with a photon index of $\Gamma \approx 0.5$ below a sharp cutoff at 7–10 MeV (Fig. 2). This time profile and the spectral shape suggest that the origin of the γ-ray afterglow radiation is different from that of bremsstrahlung radiation from electrons accelerated in thunderclouds[6,23] (known as 'γ-ray glows'[1]), which exhibit Gaussian-like time profiles that last for a minute and have an energy spectrum with a steeper slope of $\Gamma \approx 1$–2 and a less sharp cutoff at around 20 MeV.

After the subsecond afterglow, the count rates in the 0.35–0.60-MeV energy range from detectors A and D (Fig. 3a, b) increased for up to a minute. In Fig. 4 we show the energy spectra during this period of enhancement. The most striking feature in the spectra is a prominent emission line at about 0.51 MeV, which is in very good agreement with the energy for electron–positron annihilation of 0.511 MeV. The centre energies of the Gaussian line profiles were determined to be 0.515 ± 0.006 (stat.) ± 0.006 (syst.) MeV and 0.501 ± 0.003 (stat.) ± 0.006 (syst.) MeV for detectors A and D, respectively (where 'stat.' refers to the statistical uncertainty (1 s.d.) and 'syst.' to systematic uncertainty; see Methods section 'Instrumental calibration'). The hypothesis that the line originates from the environmental background is thus rejected because the centre energies of the environmental background of the candidate lines are either 0.583 MeV (natural radionuclide ^{208}Tl) or 0.609 MeV (^{214}Bi). The continuum is well explained by the combination of photo-absorption and Compton scattering of approximately 0.51-MeV photons, and supports the interpretation of the annihilation line being from positrons (Fig. 3).

The time profile of the annihilation signal (Fig. 3c, d) has an exponentially decaying component with a time constant of about 5 s in both detectors (A and D). A subsequent delayed component was also detected, albeit only in detector A, with a profile that is fitted by a Gaussian with a peak at $t_{peak} = 34.5 \pm 1.0$ s and a width of 13.2 ± 1.0 s (1σ).

We next investigate the mechanism for producing the positrons. A potential scenario is that electron–positron pairs are produced by high-energy γ-rays in the electron acceleration process[2,3]. However, the annihilation signal (Figs 3 and 4) was not accompanied by such 'seed' γ-rays, which have energies of more than 3 MeV. In addition, the environmental electric field that was measured on the ground was upwards during the annihilation signal (and less than about -3 kV m^{-1}) and so positrons should not have accumulated towards the ground and the annihilation line should not have been enhanced. Consequently, the most straightforward interpretation of the data are photonuclear reactions[15–19] (see Methods section 'Neutrons from lightning and thunderstorms'): a burst (or flash) of the lightning-triggered γ-ray photons (which caused the initial instrumental undershoot) collided with atmospheric nuclei and initiated nuclear reactions. The atmospheric photonuclear reactions $^{14}\mathrm{N} + \gamma \rightarrow {}^{13}\mathrm{N} + n$ and $^{16}\mathrm{O} + \gamma \rightarrow {}^{15}\mathrm{O} + n$ generate fast neutrons with a kinetic energy of $E_0 \approx 10$ MeV and unstable radioactive isotopes, which generate positrons in β^+ decays.

The fast neutrons that are produced undergo moderation and diffusion down to the epithermal energy (0.1–100 eV) via multiple elastic scatterings with atmospheric nuclei, particularly nitrogen (see Methods

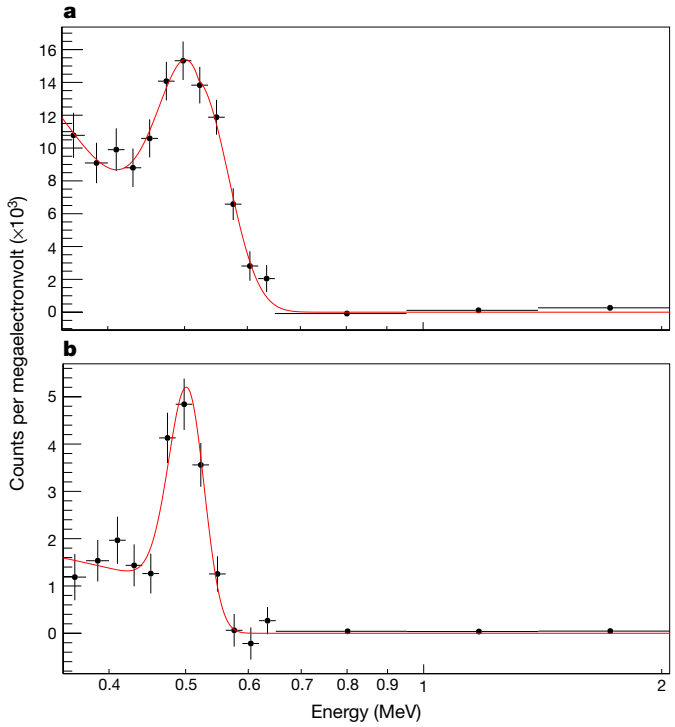

Figure 4 | γ-ray spectra during the prolonged annihilation signal. **a**, Detector A. **b**, Detector D. The error bars show $\pm 1\sigma$. Events are accumulated over the time regions described in Fig. 3 and the background spectra are subtracted from the same time span as in Fig. 2. The spectra are shown without removing the response of the detectors. Red curves show the best-fitting empirical models, consisting of a Gaussian line profile plus a power-law continuum, the latter representing the Compton-scattering component from the former (see Methods section 'Positrons and annihilation'). Gaussian widths are consistent with the energy resolution of the instruments (Extended Data Table 1).

section 'Neutron propagation'). During this process, 96% of neutrons disappear via the production of charged particles ($^{14}N + n \rightarrow {}^{14}C + p$, where p denotes a proton), producing quasi-stable ^{14}C nuclei (with a half life of 5,730 years) without emitting any strong γ-rays; the other 4% are radiatively captured by atmospheric nitrogen or matter on the ground, including that around detectors. The nuclei that capture a neutron promptly emit multiple de-excitation γ-ray lines, such as $^{14}N + n \rightarrow {}^{15}N + \gamma$. The theoretical capture rate decays exponentially with a timescale of 56 ms, which is consistent with the decay constants of 40–60 ms that were observed in the subsecond afterglow. The simulated de-excitation γ-ray spectra for our detectors, which are determined taking into account the atmosphere, surrounding materials and energy resolution of the detector, are also found to be consistent with the observed data (Fig. 2). Notably, the sharp cutoff at about 10 MeV can be explained by the lack of nuclear lines above this energy (see Methods section 'Neutron capture').

The other main products, ^{13}N and ^{15}O, decay gradually into stable ^{13}C and ^{15}N nuclei via β^+ decays: $^{13}N \rightarrow {}^{13}C + e^+ + \nu_e$ (half life, 598 s) and $^{15}O \rightarrow {}^{15}N + e^+ + \nu_e$ (half life, 122 s), respectively, where e^+ denotes a positron and ν_e an electron neutrino. A region, or 'cloud', filled with these isotopes emits positrons for more than 10 min and moves by wind above our detectors without experiencing much diffusion, owing to a low mobility of the isotopes. A positron emitted from ^{13}N or ^{15}O travels a few metres in the atmosphere, annihilates quickly in meeting an ambient electron and radiates two 0.511-MeV photons, the atmospheric mean free path of which is about 89 m. This process produced the delayed annihilation component that was detected at $t = 11$–63 s with detector A. The epoch t_{peak} is consistent with the wind velocity and direction on the day (see Fig. 1 and Methods section 'Ambient wind flow'). The decaying phase ($t < 10$ s) observed with detectors A and D is interpreted as a consequence of photonuclear reactions in the vicinity of the detectors (see Methods section 'Decaying annihilation signal'). We note that we detected a similar annihilation signal once before[22]; however, the result was marginal at best, mainly because measurement of the neutron signal was hampered by the initial instrumental undershoot (see Methods section 'Comparison with a similar event').

Here we estimate quantitatively the total yield of the reactions from the delayed annihilation signal observed at detector A ($t = 11$–63 s; Fig. 3c). We find using Monte Carlo simulations that the annihilation spectrum can be interpreted as the result of emission that underwent atmospheric absorption and scattering by 80-m-thick air between the cloud base and the detector (see Methods section 'Positrons and annihilation'). Because the number of delayed 0.511-MeV photons is $N_{511} = (1.4 \pm 0.2) \times 10^3$ during the observation period $\Delta t = 52$ s, the corresponding time-integrated β^+-decay density for the period is estimated to be $n_{\beta+} = 3.1 \times 10^{-3}$ cm^{-3}, assuming a simplified cylindrical volume V for the cloud with a horizontal radius of $R_d = 220$ m (see Methods section 'Ambient wind flow') and fiducial vertical discharge length of $L_d = 1$ km (refs 25–27). Taking into account the contributions from ^{13}N and ^{15}O (see Methods section 'Contribution from oxygen'; for example, positrons emitted by ^{15}O amounts 44% of those emitted by ^{13}N at $t_{peak} = 35$ s), the initial total number density of isotopes ^{13}N and ^{15}O is derived to be $n_0 = 2.6 \times 10^{-2}$ cm^{-3}. Consequently, the total number of neutrons produced is

$$N_n = n_0 V = 4 \times 10^{12} \left(\frac{R_d}{220\ \mathrm{m}} \right)^2 \left(\frac{L_d}{1.0\ \mathrm{km}} \right)$$

which is within the range of $N_n = 10^{11-15}$ predicted theoretically from studies[17,19] of the terrestrial γ-ray flash.

There are only two known natural origins of carbon isotopes on Earth: stable primordial ^{13}C from geological time, which originated from stellar nucleosynthesis[28], and semi-stable ^{14}C, which is produced via atmospheric interactions with cosmic rays. The lightning-triggered atmospheric nuclear reactions provide a previously unknown channel for generating isotopes of carbon, nitrogen and oxygen (^{13}C, ^{14}C, ^{13}N, ^{15}N and ^{15}O) naturally on Earth. The short-lived isotopes ^{13}N and ^{15}O provide a new methodology for studying lightning, via positrons observed from the ground. The more stable ^{13}C, ^{14}C and ^{15}N isotopes contribute to the natural isotope composition on Earth, albeit only a small fraction.

Online Content Methods, along with any additional Extended Data display items and Source Data, are available in the online version of the paper; references unique to these sections appear only in the online paper.

Received 30 July; accepted 10 October 2017.

1. Dwyer, J. R., Smith, D. M. & Cummer, S. A. High-energy atmospheric physics: terrestrial gamma-ray flashes and related phenomena. *Space Sci. Rev.* **173,** 133–196 (2012).
2. Gurevich, A. V., Milikh, G. M. & Roussel-Dupré, R. Runaway electron mechanism of air breakdown and preconditioning during a thunderstorm. *Phys. Lett. A* **165,** 463–468 (1992).
3. Dwyer, J. R. The relativistic feedback discharge model of terrestrial gamma ray flashes. *J. Geophys. Res.* **117,** A02308 (2012).
4. Torii, T., Takeishi, M. & Hosono, T. Observation of gamma-ray dose increase associated with winter thunderstorm and lightning activity. *J. Geophys. Res.* **107,** 4324 (2002).
5. Dwyer, J. R. *et al.* A ground level gamma-ray burst observed in association with rocket-triggered lightning. *Geophys. Res. Lett.* **31,** L05119 (2004).
6. Tsuchiya, H. *et al.* Detection of high-energy gamma rays from winter thunderclouds. *Phys. Rev. Lett.* **99,** 165002 (2007).
7. Chilingarian, A. *et al.* Ground-based observations of thunderstorm-correlated fluxes of high-energy electrons, gamma rays, and neutrons. *Phys. Rev. D* **82,** 043009 (2010).
8. Dwyer, J. R. *et al.* Observation of a gamma-ray flash at ground level in association with a cloud-to-ground lightning return stroke. *J. Geophys. Res.* **117,** A10303 (2012).
9. Tsuchiya, H. *et al.* Observation of thundercloud-related gamma rays and neutrons in Tibet. *Phys. Rev. D* **85,** 092006 (2012).

10. Dwyer, J. R. *et al.* Positron clouds within thunderstorms. *J. Plasma Phys.* **81,** 475810405 (2015).
11. Fishman, G. J. *et al.* Discovery of intense gamma-ray flashes of atmospheric origin. *Science* **264,** 1313–1316 (1994).
12. Smith, D. M., Lopez, L. I., Lin, R. P. & Barrington-Leigh, C. P. Terrestrial gamma-ray flashes observed up to 20 MeV. *Science* **307,** 1085–1088 (2005).
13. Tavani, M. *et al.* Terrestrial gamma-ray flashes as powerful particle accelerators. *Phys. Rev. Lett.* **106,** 018501 (2011).
14. Briggs, M. S. *et al.* First results on terrestrial gamma ray flashes from the Fermi Gamma-ray Burst Monitor. *J. Geophys. Res.* **115,** A07323 (2010).
15. Babich, L. P. Generation of neutrons in giant upward atmospheric discharges. *Sov. JETP Lett.* **84,** 285–288 (2006).
16. Babich, L. P. Neutron generation mechanism correlated with lightning discharges. *Geomagn. Aeron.* **47,** 664–670 (2007).
17. Carlson, B. E., Lehtinen, N. G. & Inan, U. S. Neutron production in terrestrial gamma ray flashes. *J. Geophys. Res.* **115,** A00E19 (2010).
18. Babich, L. P., Bochkov, E. I., Kutsyk, I. M. & Rassoul, H. K. Analysis of fundamental interactions capable of producing neutrons in thunderstorms. *Phys. Rev. D* **89,** 093010 (2014).
19. Babich, L. P., Bochkov, E. I., Kutsyk, I. M. & Roussel-Dupré, R. A. Localization of the source of terrestrial neutron bursts detected in thunderstorm atmosphere. *J. Geophys. Res.* **115,** A00E28 (2010).
20. Shah, G. N., Razdan, H., Ali, Q. M. & Bhat, C. L. Neutron generation in lightning bolts. *Nature* **313,** 773–775 (1985).
21. Gurevich, A. V. *et al.* Strong flux of low-energy neutrons produced by thunderstorms. *Phys. Rev. Lett.* **108,** 125001 (2012).
22. Umemoto, D. *et al.* On-ground detection of an electron-positron annihilation line from thunderclouds. *Phys. Rev. E* **93,** 021201(R) (2016).
23. Tsuchiya, H. *et al.* Long-duration γ ray emissions from 2007 and 2008 winter thunderstorms. *J. Geophys. Res.* **116,** D09113 (2011).
24. Hare, B. M. *et al.* Ground-level observation of a terrestrial gamma ray flash initiated by a triggered lightning. *J. Geophys. Res.* **121,** 6511–6533 (2016).
25. Rakov, V. A. & Uman, M. A. *Lightning: Physics and Effects* (Cambridge Univ. Press, 2003).
26. Chen, L., Zhang, Q., Hou, W. & Tao, Y. On the field-to-current conversion factors for large bipolar lightning discharge events in winter thunderstorms in Japan. *J. Geophys. Res.* **120,** 6898–6907 (2015).
27. Wu, T. *et al.* Large bipolar lightning discharge events in winter thunderstorms in Japan. *J. Geophys. Res.* **119,** 555–566 (2014).
28. Woosley, S. E. & Weaver, T. A. The evolution and explosion of massive stars. II. Explosive hydrodynamics and nucleosynthesis. *Astrophys. J. Suppl. Ser.* **101,** 181–235 (1995).

Acknowledgements We thank the members of the radiation safety group of the Kashiwazaki-Kariwa nuclear power station, TEPCO Inc., for providing observation sites, H. Miyahara, N. Kawanaka and H. Ohgaki for discussions, H. Sakurai, M. Niikura and the Sakurai group members at RIKEN Nishina Center for providing $Bi_4Ge_3O_{12}$ scintillation crystals, T. Tamagawa for project support, G. Bowers, M. Kamogawa and D. Smith for suggestions on our interpretation, S. Otsuka and H. Kato for supporting the detector developments, and the RIKEN Advanced Center for Computing and Communication for use of the HOKUSAI GreatWave supercomputing system for Monte Carlo simulations. This research is supported by JSPS/MEXT KAKENHI grant numbers 15K05115, 15H03653 and 16H06006, by SPIRITS 2017 and Hakubi projects of Kyoto University, and by the joint research programme of the Institute for Cosmic Ray Research (ICRR), The University of Tokyo. Our project is also supported by crowdfunding ('Thundercloud Project', using the academic crowdfunding platform 'academist'), and we are grateful to Y. Shikano, Y. Araki, M. T. Hayashi, N. Matsumoto, T. Enoto, K. Hayashi, S. Koga, T. Hamaji, Y. Torisawa, S. Sawamura, J. Purser, S. Suehiro, S. Nakane, M. Konishi, H. Takami, T. Sawara and all of the backers of Thundercloud Project. We are grateful to M. Sakano of Wise Babel Ltd for linguistic help and to the 'adachi design laboratory' for supporting the crowdfunding acvitity. The background image in Fig. 1 was provided by the Geospatial Information Authority of Japan.

Author Contributions T.E., Y.W., Y.F., K.O., K.N., T.Y., T.N. and H.T. were responsible for the detector developments, data analyses and interpretation; T.E. is the project leader and wrote the draft of the manuscript; Y.W. made a major contribution to the detector development, installation and, in particular, analysis; Y.F. led the Monte Carlo simulations using Geant4; K.N. led the installation of the instruments at Kashiwazaki-Kariwa in 2016 and the laboratory experiment outlined in Methods section 'Initial flash'; T.Y. led the development of the new data acquisition system after 2015; D.U. provided the data from 2012; and M.S., Y.S., K.M. and H.T. contributed to the data interpretation.

Author Information Reprints and permissions information is available at www.nature.com/reprints. The authors declare no competing financial interests. Readers are welcome to comment on the online version of the paper. Publisher's note: Springer Nature remains neutral with regard to jurisdictional claims in published maps and institutional affiliations. Correspondence and requests for materials should be addressed to T.E. (teruaki.enoto@gmail.com).

Reviewer Information *Nature* thanks L. Babich and the other anonymous reviewer(s) for their contribution to the peer review of this work.

METHODS

GROWTH collaboration. Winter thunderstorms along the coast of the Sea of Japan are much feared natural phenomena for the locals[25]. For the same reasons, in the winter season the area is ideal for observing high-energy phenomena from lightning and thunderclouds: powerful thunderstorms are frequent, and the cold temperatures lower the cloud-base altitude[25,29] to 0.2–0.8 km, which means that any γ-rays emitted from them reach the ground easily. The Gamma-Ray Observation of Winter Thunderclouds (GROWTH) project is a collaboration developed to study the high-energy radiation from lightning and thunderstorms, starting in 2006[6,23]. The site of our experiment, Kashiwazaki-Kariwa nuclear power station, is located at 37.4267° N, 138.6014° E and at an altitude of about 30–40 m. The detectors that operated during the winter in 2016–2017 are summarized in Extended Data Table 1. Detectors A–C were newly deployed in 2016; they use a 25 cm × 8 cm × 2.5 cm $Bi_4Ge_3O_{12}$ (BGO) scintillation crystal, with two photomultiplier tubes (PMTs; HAMAMATSU R1924A) attached to for each. Signals are read out via analogue circuits connected to an analogue-to-digital converter (ADC) board developed with crowdfunding support. Detector D has been in operation since 2010 and consists of a 7.62 cm (height) × 7.62 cm (diameter) NaI scintillation crystal with a PMT R6231 attached to it. Signals for detector D are read out via another analogue circuit. In each detector, individual radiation events are recorded with time and pulse height. The effective areas are determined to be 149 cm^2 and 28 cm^2 at 0.511 MeV for detectors A–C and D, respectively; in the Monte Carlo simulation using Geant4[30], irradiated photons are monochromatic at 0.511 MeV. The environmental electric field was monitored at the position of detector D.

Lightning discharges. On 6 February 2017, the Japan lightning-detection network, operated by Franklin Japan Co. Ltd, recorded a pair of cloud-to-ground lightning discharges. A negative discharge at 08:34:06.002716165 UTC with a peak current of −33 kA was reported, followed by a positive one 23.7 μs later with a peak current of +44 kA. The positions indicated in the report are marked by '−' and '+' in Fig. 1a. An associated electromagnetic signal was confirmed in the frequency range 1–100 Hz at the Kuju station (33.059° N, 131.233° E) in Japan, which is located about 830 km southwest from the position of the lightning (Extended Data Fig. 1). This observation supports the hypothesis that the two discharges occurred simultaneously for this event. An unequivocal determination of the types of the discharges is left for future work, because the data presented here are insufficient to investigate the possibility of misidentification of bipolar discharges, which occur frequently in this area[31,32].

Initial flash. All of the detectors (A–D) recorded a strong bursting event coincidentally with the lightning within instrumental uncertainties of the time tagging of the event (see Methods section 'Instrumental calibration'; Fig. 1). Detectors A–C digitize the waveform of an analogue pulse of the PMT output for 20 μs once the pulse height exceeds the trigger threshold, and record the highest and lowest values. The former is used to measure the energy of the pulse signal and the latter can be used to monitor the analogue baseline voltage. In contrast, detector D does not provide direct information on the baseline voltage, which is crucial in this case, as discussed below. For that reason, we exclude the data from detector D for the first 1 s of the event in our analysis.

At the initial stage of the recorded event, we noticed that the baseline voltages were very negative. The level of the baseline gradually settled down to the nominal value in 20–40 ms (Extended Data Fig. 2). This is abnormal and cannot be a technical glitch in the system because the detectors are completely separate and located hundreds of metres apart from one another.

The most plausible interpretation is that the detectors received an extremely strong signal with an intensity beyond the maximum that they are able to measure, lasting for much shorter than 1 ms, which caused the peculiar analogue undershoot that lasted for about 10 ms. At the laboratory we conducted follow-up experiments using detectors A–C. We applied a bias voltage of 1,100 V, which is higher than that set during the field observation (about 900 V), to raise the PMT gain by a factor of about 5. In this configuration, a cosmic-ray muon-penetration signal equivalent to a 30–50-MeV energy deposit is amplified to a 150–250-MeV γ-ray-equivalent charge output. We observed the 'peculiar' undershoot with an intensity up to −1,000 in the ADC channel and a recovery time constant of about 1 ms, both of which are very similar to what were observed in the lightning event by detectors B and C. This result confirms our interpretation; there must have been an initial strong radiation flash at the time of the lightning, even though it was not measured with our detectors directly.

In detector A, the undershoot lasted longer than in detectors B and C. The level of the undershoot at $t = 40$ ms is equivalent to an energy shift of about −0.5 MeV, which changes the energy scale by more than 50% below 1 MeV, but only by about 5% at 10 MeV. To minimize the effect of this energy-scale shift, we extracted and plotted spectra of the subsecond afterglow above 1 MeV in Fig. 2.

Radiation monitors. Radiation monitors are installed at the site at 300–400 m intervals (Fig. 1) and are operated at all times. Each radiation monitor has a spherical ion chamber filled with about 14 litres of argon gas, and covers an energy range above 3 MeV with a coarse time resolution of 30 s.

Instrumental calibration. Energy calibrations were performed by a linear fitting of the persistent environmental background emission lines (see, for example, Fig. 2) of ^{40}K (1.461 MeV) and ^{208}Tl (2.615 MeV). We performed this calibration procedure for detectors A–C every 30 min to correct the sensitive temperature dependence of light yields of the BGO scintillation crystals (about 1% per degree Celsius), whereas we did it daily for the NaI of detector D. We evaluated the uncertainty of this energy calibration using another background emission line, of ^{214}Bi at 0.609 MeV, which appears with rainfall as a component of radon wash-out radiation. The measured centre energy fluctuates around 0.609 MeV with a standard deviation of 0.007 MeV. Thus, the energies of individual photons are calibrated to an accuracy of 1.1% (systematic uncertainty), about 0.006 MeV for 0.511 MeV, in all detectors (A–D).

The relative timing tags of detectors A–C have 2-μs resolution for each photon, which is the typical timescale of the analogue signal waveforms. Absolute timing tags are usually assigned from the Global Positioning System (GPS) signals. Because the signal was lost during the event on 6 February, we instead referred to the internal clock time (Unix time) and confirmed only that the rising edges of the initial flash were recorded within 1 s of the lightning.

Hence, we further calibrated the absolute timing of detectors A–C by assuming that the rising edge of the initial flash was synchronized with the lightning. Detector D has a 100-μs relative time resolution for each photon, with time assignment from GPS signals received during the event. Because the rising edge of detector D was consistent with the lightning to within about 10 ms, we did not perform additional timing correction. However, further detailed comparison of the relative timing between the initial flash and the lightning is beyond the present accuracy of absolute timing calibration.

Neutrons from lightning and thunderstorms. Historically, experiments have been performed with the aim of detecting neutrons generated from nuclear fusion (deuteron–deuteron reactions) in lightning and thunderstorms[20,33–35]. More recently, photonuclear reactions have been theoretically suggested to be a plausible physical process in lightning[10,15–19]. Although enhancements of the neutron flux in thunderstorms[7,21,36] have generally been thought to be observational evidence of photonuclear reactions, their atmospheric origin is still debated owing to the experimental difficulty of discriminating the radiation signatures for those reactions from contamination of bremsstrahlung γ-rays[9,37–39].

Neutron propagation. The physical processes that follow the photonuclear reactions are illustrated schematically in Extended Data Fig. 3. The photonuclear reactions $^{14}N + \gamma \rightarrow {}^{13}N + n$ and $^{16}O + \gamma \rightarrow {}^{15}O + n$ expel fast neutrons from atmospheric nitrogen and oxygen. The kinetic energy of the photo-neutrons is distributed up to $E_\gamma - E_{th}$, where E_γ and E_{th} are the incident photon energy and photonuclear threshold energy ($E_{th} \approx 10$ MeV; refs 10, 17–19), respectively. In the following discussion, we consider only the most abundant target, ^{14}N, because the neutron cross-section with the second most abundant target (^{16}O) is relatively small. The neutron cross-section with ^{14}N, shown in Extended Data Fig. 4a, has three main processes: elastic scattering, charged-particle production $^{14}N + n \rightarrow {}^{14}C + p$ and radiative neutron capture $^{14}N + n \rightarrow {}^{15}N + \gamma$. Incident fast neutrons lose their kinetic energy gradually via multiple elastic scatterings, the cross-section of which is almost independent of energy, $\sigma_{es} \approx 10$ barns (refs 40 and 41) for 10^{-2}–10^4 eV, and is much larger than those of the other two processes. As neutrons are moderated and diffuse to the epithermal energy (0.1–100 eV), the cross-sections of charged-particle production and neutron capture increase gradually, and neutrons disappear.

The neutron moderation occurs in a similar situation to some nuclear engineering[42]. Let lethargy ξ be the logarithm of the inverse ratio of the change in neutron kinetic energy in a single elastic scattering (from E_n to E_{n+1}, where E_n is the energy after n scatterings). It is approximated as $\xi = \ln(E_n/E_{n+1}) \approx 2/(A + 2/3) = 0.136$, where $A = 14$ is the mass number of nitrogen. Because the energy deposit in a single scattering is $\Delta E = E_n - E_{n+1} = (1 - e^{-\xi})E_n = 0.127E_n$, the neutron energy decreases from the initial energy E_0 as $E_n = 0.873^n E_0$. Between contiguous scattering events, the mean free path λ is almost independent of the neutron energy[42]:

$$\lambda = 23.8\ \mathrm{m}\left(\frac{\sigma_{es}}{10\ \mathrm{barns}}\right)^{-1}\left(\frac{\rho}{10^{-3}\ \mathrm{g\ cm^{-3}}}\right)^{-1}\left(\frac{A}{14}\right)^{-1}$$

where ρ is the atmospheric nitrogen density. The duration between the two contiguous scatterings is $\Delta t_n = \lambda\sqrt{m_n/(2E_n)}$, where $m_n = 940$ MeV is the neutron rest-mass energy. The elapsed time until the nth scattering is $t_n = \sum_{n'} \Delta t_{n'}$. The number of neutrons N_n decreases as a result of absorption by nitrogen nuclei; the loss of N_n in the nth scattering is $\Delta N_n = N_{n-1}\{1 - \exp[-(\sigma_{np} + \sigma_{cap})/\sigma_{es}]\}$, where

σ_{np} and σ_{cap} are the cross-sections of charged-particle production and neutron capture, respectively. Numerically solving for E_n, t_n and ΔN_n with n (Extended Data Fig. 4b), the number of the surviving neutrons at t for 5–120 ms is approximately $N(t) = N(0)\exp(-t/\tau_n)$, with decay constant $\tau_n = 56$ ms. Therefore, the neutron disappearing rate via capture is

$$\frac{dN_{cap}}{dt} = \frac{\sigma_{cap}}{\sigma_{np}+\sigma_{cap}}\frac{dN(t)}{dt} \propto \exp\left(-\frac{t}{\tau_n}\right)$$

The theoretical ($\tau_n \approx 56$ ms) and observed (40–60 ms) decay constants are found to be consistent with each other. In addition, assuming isotropic random-walk scatterings, the diffusion distance λ_D is estimated to be

$$\begin{aligned}\lambda_D &= \sqrt{6Dt}\\ &\approx \sqrt{6(\lambda\nu)t} = \sqrt{6\lambda^2\nu t/\lambda}\\ &\approx \lambda\sqrt{6n} = 639\ \mathrm{m}\left(\frac{\lambda}{23.8\ \mathrm{m}}\right)\left(\frac{n}{120}\right)^{1/2}\end{aligned}$$

where D and ν are the diffusion coefficient and velocity of neutrons in the atmosphere, respectively. The diffusion scale is the same order of magnitude as the distance between our detectors and the lightning discharges (0.5–1.7 km) for $n = 100$–140 scatterings (Extended Data Fig. 4b).

Neutron capture. Moderated neutrons are captured by nuclei in the atmosphere, surrounding materials and detectors. The nucleus then promptly radiates several γ-ray photons at discrete energies below about 10 MeV within nanoseconds. We simulated the expected γ-ray spectra with Geant4 Monte Carlo simulations. We implemented the BGO scintillation crystals, the aluminium plates of the supporting jigs, a detector box made of acrylonitrile butadiene styrene resin and polycarbonate, and lead blocks below. The detectors were placed on a 1-m-thick flat concrete base, which imitates the building, and in an atmosphere with a uniform density of 1.2×10^{-3} g cm^{-3}, composed of nitrogen (75.527% weight fraction), oxygen (23.145%), argon (1.283%) and carbon dioxide (0.045%). De-excitation γ-rays with an energy of more than 0.1 MeV and branching ratio of more than 10% of the strongest line were generated isotropically and uniformly from atmospheric nitrogen (^{14}N), surrounding materials (^{27}Al, ^{28}Si and ^{207}Pb) and the $Bi_4Ge_3O_{12}$ crystal itself (^{70}Ge, ^{72}Ge, ^{74}Ge and ^{209}Bi) according to the branching ratios from the Evaluated Nuclear Structure Data File (ENSDF) database (http://www.nndc.bnl.gov/ensdf/). We compared the observed spectra of detectors A–C with the simulated ones (Extended Data Fig. 5) and found that a cylindrical source geometry with a horizontal radius of $R_d = 220$ m and a vertical length of $L_d = 1$ km can reproduce the spectrum from detector A. In contrast, a source about 300 m away from the detectors consisting solely of the nitrogen contribution was found to roughly reproduce the spectra from detectors B and C. These results indicate that neutrons hit matter surrounding detector A, whereas only de-excitation γ-rays from atmospheric nitrogen reached detectors B and C.

Decaying annihilation signal. The rapidly decaying annihilation signal was observed just after the discharge (Fig. 3) in detectors A and D, with a typical timescale of 5 s. This timescale is much shorter than that of the positron-emitting cloud motion and half lives of ^{13}N and ^{15}O. Therefore, we consider that photonuclear reactions with abundant materials around the detectors, such as $^{28}\mathrm{Si}+\gamma\rightarrow{}^{27}\mathrm{Si}+n$ in the soil and $^{27}\mathrm{Al}+\gamma\rightarrow{}^{26\mathrm{m}}\mathrm{Al}+n$ in the detectors or their housings, are the more plausible origins of this emission component than the positron-emitting cloud. Subsequent β^+ decays of the unstable radioisotopes, $^{27}\mathrm{Si}\rightarrow{}^{27}\mathrm{Al}+e^++\nu_e$ and $^{26\mathrm{m}}\mathrm{Al}\rightarrow{}^{26}\mathrm{Mg}+e^++\nu_e$, have half lives of 4.15 s and 6.35 s, respectively, consistent with the observed decay timescale of 5 s.

Ambient wind flow. The ambient wind flow at an altitude of 85 m was northwesterly (Fig. 1) with a velocity of $v_w = 17$ m s^{-1} and constant to within ±1 m s^{-1} during the event, according to a weather monitor near detector D operated by the nuclear power station. The wind information was also confirmed by using weather radar images from the Japan Meteorological Agency (Extended Data Fig. 1b–d). The time profile of the delayed annihilation signal (Fig. 3c) is approximated by a Gaussian with a peak time of $t_{peak} = 34.5\pm1.0$ s and a duration of $\sigma_t = 13.2\pm1.0$ s (1σ). The drifting distance of the positron-emitting cloud during the period 0–t_{peak} is then calculated to be $v_w t_{peak} \approx 590$ m. This distance is comparable with the separation between detector A and the location of the discharges. The wind direction is also consistent with our interpretation. A typical horizontal size (radius) of the cloud is estimated from the duration to be

$$R_d = v_w\sigma_t \approx 220\ \mathrm{m}\left(\frac{v_w}{17\ \mathrm{m\ s^{-1}}}\right)\left(\frac{\sigma_t}{13.2\ \mathrm{s}}\right)$$

Positrons and annihilation. Here we examine positron emission from radioactive isotopes and 0.511-MeV annihilation line emission. Positrons are emitted isotropically with continuous energy spectra following the β^+ formula with maximum kinetic energies of 1.19 MeV and 1.72 MeV from ^{13}N and ^{15}O, respectively. Roughly 97% of positrons with an initial kinetic energy of about 1 MeV annihilate with non-relativistic electrons via positronium formation, after losing their kinetic energy within a few metres by ionizing ambient atoms, and subsequently emit two 0.511 MeV photons back-to-back. The remaining 3% annihilate directly in flight (direct annihilation of relativistic positrons[43]) and emit two photons with energies between about $m_ec^2/2$ and $E+3m_ec^2/2$, where m_ec^2 and E are the rest mass and kinetic energies of positron, respectively. These photons from direct annihilation by nitrogen- and oxygen-originating positrons make a weak continuum up to about 2.0 MeV and 2.5 MeV, respectively.

To examine the expected spectrum from annihilation processes, we performed Geant4 Monte Carlo simulations using a setup similar to that for the de-excitation γ-ray simulations. We assumed a cylindrical positron-emitting cloud with various distances to its base. Positrons were generated isotropically and uniformly inside the source volume, with a continuum energy distribution of the β^+ decay, taking into account the proportion of the contributions from ^{13}N and ^{15}O. Extended Data Fig. 6 shows the resultant simulated spectra. We then compared this simulation with the observed delayed annihilation signal and found that the model with a cloud-base distance of 80 m best reproduces the observed data. Using this distance, we calculated the conversion factor for the number of β^+ decays in a unit volume to the detected annihilation photons at the 0.511-MeV line to be $N_{511}/n_{\beta+} = 4.5\times10^5$ cm^3, assuming the horizontal radius $R_d = 220$ m (see Methods section 'Ambient wind flow'). The total number of β^+ decay events in a unit volume is calculated to be $n_{\beta+} = 3.1\times10^{-3}$ cm^{-3} from the observed number of delayed annihilation signals $N_{511} = 1.4\times10^3$.

Contribution from oxygen. Dominant targets of the atmospheric photonuclear reactions are ^{14}N and ^{16}O. The incident γ-ray spectrum is assumed to have the same shape as that in the previously reported terrestrial γ-ray flashes: $N(E)\propto E^{-\Gamma}\exp(-E/E_c)$ for photon energy E, photon index $\Gamma = 1.4$ and cutoff energy $E_c = 6.6$ MeV (ref. 13). The event-number ratio η_{prod} of the photonuclear reactions with ^{16}O to those with ^{14}N is estimated to be $\eta_{prod} = 10.4\%$, when integrated over the energies of seed γ-rays up to about 28 MeV, using the atmospheric abundances of nitrogen (78.08%) and oxygen (20.94%) and the experimental cross-sections (about 15 mb and 10 mb for ^{14}N and ^{16}O at about 23 MeV, respectively[40]). The event rates per unit time of the subsequent β^+ decays also differ, owing to a difference in the half lives: 597.9 s and 122.2 s (decay constants of $\lambda_{13N} = 1.16\times10^{-3}$ s^{-1} and $\lambda_{15O} = 5.67\times10^{-3}$ s^{-1}) for ^{13}N and ^{15}O, respectively. These give the decay rates to be $dN_{13N}(t)/dt = \lambda_{13N}\exp(-\lambda_{13N}t)$ and $dN_{15O}(t)/dt = \lambda_{15O}\exp(-\lambda_{15O}t)$ for ^{13}N and ^{15}O, respectively. Therefore, the ratio of the contribution of the annihilation signal of the positrons from ^{15}O to that from ^{13}N is

$$\begin{aligned}\eta(t) &= \eta_{prod}\frac{dN_{15O}(t)/dt}{dN_{13N}(t)/dt}\\ &= \eta_{prod}\frac{\lambda_{15O}}{\lambda_{13N}}\exp[-(\lambda_{15O}-\lambda_{13N})t]\\ &= 0.51\exp\left(-\frac{t}{222\ \mathrm{s}}\right)\end{aligned}$$

yielding about 44% at $t_{peak} = 35$ s. Using the number densities n_{13N} and n_{15O} of ^{13}N and ^{15}O, respectively, the β^+ decay rate is $S_{\beta+}(t) = \lambda_{13N}n_{13N}(t) + \lambda_{15O}n_{15O}(t)$. Combining the above estimates with the relation $S_{\beta+}\Delta t = n_{\beta+}$, where $\Delta t = 52$ s and $n_{\beta+} = 3.1\times10^{-3}$ cm^{-3}, we derive $n_{13N} = 1.6\times10^{-2}$ cm^{-3} at t_{peak} and an initial number density of isotopes of $n_0 = n_{13N}(0) + n_{15O}(0) = 2.6\times10^{-2}$ cm^{-3}.

Comparison with a similar event. An event associated with 0.511-MeV emission, similar to the event reported here, was detected previously at the same site on 13 January 2012[22]. At the time of that event, only detector D was operated. The data acquisition was heavily hampered by the analogue undershoot for about 200 ms; thus studying the subsecond afterglow with de-excitation spectra was impossible. In addition, because the electric-field monitor was not working at that time, we were unable to eliminate the pair-production scenario entirely. In contrast, in the event reported here, we measured the environmental electric field at detector D using a commercial electric-field mill (BOLTEK EFM-100) and found it to be negative during the delayed annihilation phase, which implies that electrons moved to the ground away from negatively charged clouds. Generating the 0.511-MeV line without emitting 10–20-MeV bremsstrahlung photons is thus impossible.

Data and code availability. The data for Himawari 8 in Extended Data Fig. 1a were obtained from the Science Cloud of the National Institute of Information

and Communications Technology (NICT), Data Integration and Analysis System Program (DIAS) by The University of Tokyo, Center for Environmental Remote Sensing (CEReS) of Chiba University and Earth Observation Research Center of Japan Aerospace Exploration Agency (https://himawari8.nict.go.jp). The data in Extended Data Fig. 1b–d were supplied by the Japan Meteorological Agency and downloaded from the website of the Research Institute for Sustainable Humanosphere, Kyoto University (http://database.rish.kyoto-u.ac.jp/index-e.html). Other datasets generated and analysed during this study are available from the corresponding author on reasonable request.

29. Goto, Y. & Narita, K. Observations of winter lightning to an isolate tower. *Res. Lett. Atmos. Elect.* **12,** 57–60 (1992).
30. Agostinelli, S. *et al.* Geant4 — a simulation toolkit. *Nucl. Instrum. Methods A* **506,** 250–303 (2003).
31. Rakov, V. A. A review of positive and bipolar lightning discharges. *Bull. Am. Meteorol. Soc.* **84,** 767–776 (2003).
32. Narita, K., Goto, Y., Komuro, H. & Sawada, S. Bipolar lightning in winter at Maki, Japan. *J. Geophys. Res.* **94,** 13191–13195 (1989).
33. Fleischer, R. L. Search for neutron generation by lightning. *J. Geophys. Res.* **80,** 5005–5009 (1975).
34. Shyam, A. & Kaushik, T. C. Observation of neutron bursts associated with atmospheric lightning discharge. *J. Geophys. Res.* **104,** 6867–6869 (1999).
35. Ishtiaq, P. M., Mufti, S., Darzi, M. A., Mir, T. A. & Shah, G. N. Observation of 2.45 MeV neutrons correlated with natural atmospheric lightning discharges by lead-free Gulmarg neutron monitor. *J. Geophys. Res.* **121,** 692–703 (2016).
36. Kuroda, Y. *et al.* Observation of gamma ray bursts at ground level under the thunderclouds. *Phys. Lett. B* **758,** 286–291 (2016).
37. Babich, L. P., Bochkov, E. I., Dwyer, J. R., Kutsyk, I. M. & Zalyalov, A. N. Numerical analysis of 2010 high-mountain (Tien-Shan) experiment on observations of thunderstorm-related low-energy neutron emissions. *J. Geophys. Res.* **118,** 7905–7912 (2013).
38. Babich, L. P., Bochkov, E. I., Kutsyk, I. M. & Zalyalov, A. N. On amplifications of photonuclear neutron flux in thunderstorm atmosphere and possibility of detecting them. *Sov. JETP Lett.* **97,** 291–296 (2013); erratum **97,** 505 (2013); erratum **99,** 242 (2014).
39. Chilingarian, A., Bostanjyan, N., Karapetyan, T. & Vanyan, L. Remarks on recent results on neutron production during thunderstorms. *Phys. Rev. D* **86,** 093017 (2012).
40. International Atomic Energy Agency. *Handbook on Photonuclear Data for Applications: Cross-sections and Spectra: Final Report of a Co-ordinated Research Project 1996–1999* 52–75 (IAEA, 2000).
41. Shibata, K. *et al.* JENDL-4.0: a new library for nuclear science and engineering. *J. Nucl. Sci. Technol.* **48,** 1–30 (2011).
42. Lamarsh, J. R. & Baratta, A. J. *Introduction to Nuclear Engineering* 3rd edn, Ch. 3 (IAEA, 2001).
43. Prantzos, N. *et al.* The 511 keV emission from positron annihilation in the Galaxy. *Rev. Mod. Phys.* **83,** 1001–1056 (2011).

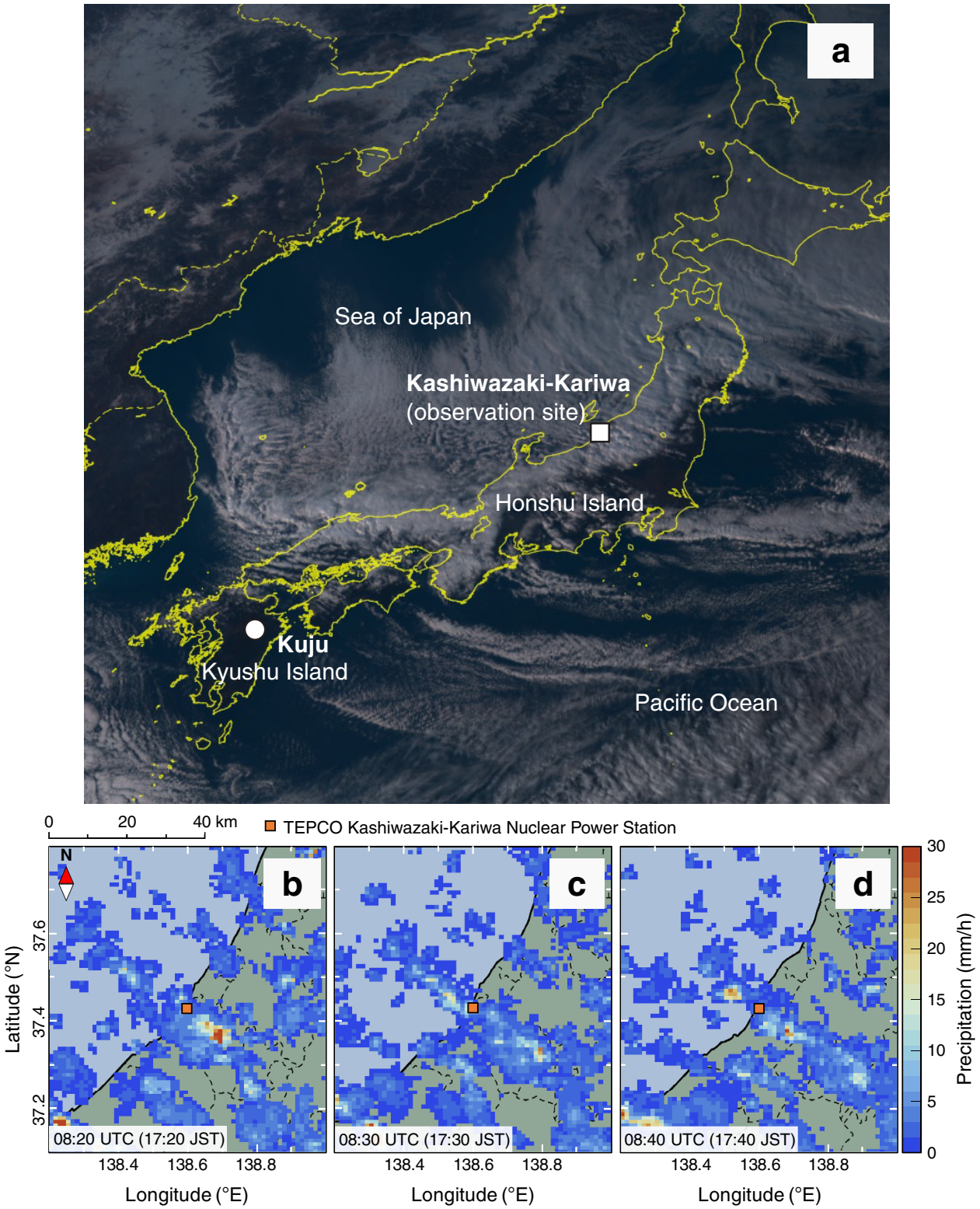

Extended Data Figure 1 | Location of the observation sites. a, Visible image of the geostationary satellite Himawari 8 at 06:00 UTC on 6 February 2017. The square and circle indicate Kashiwazaki-Kariwa and Kuju, respectively. **b–d**, Precipitation intensity map between 08:20 and 08:40 UTC on the same day, retrieved from the radar system of the Japan Meteorological Agency. Orange squares indicate Kashiwazaki-Kariwa nuclear power station.

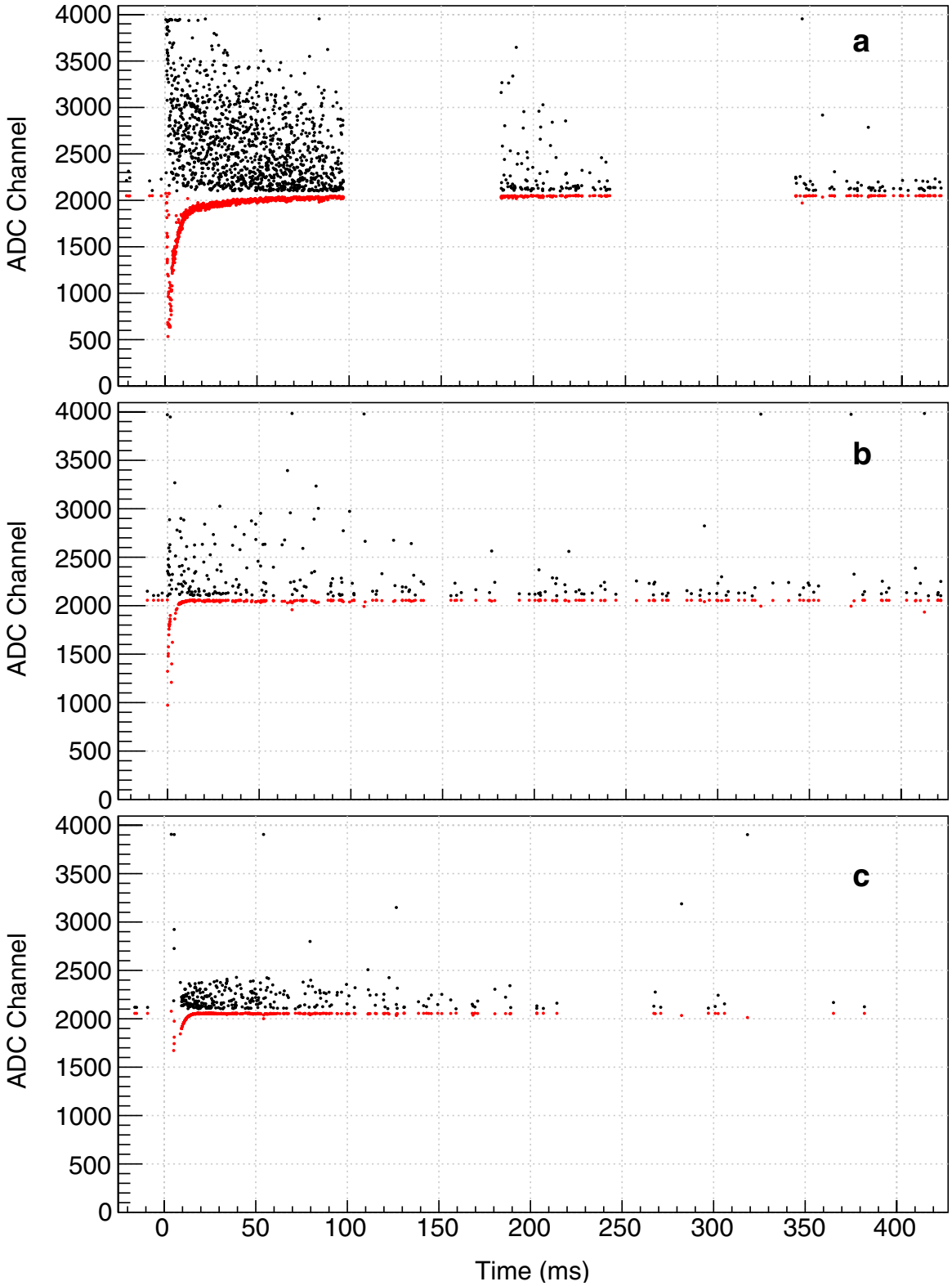

Extended Data Figure 2 | Detector response to the initial radiation flash. a–c, Time histories of the maximum (black) and minimum (red) ADC values in the ADC-sampled waveforms of the photons detected with detectors A (**a**), B (**b**) and C (**c**). Normally, the minimum value is equal to the baseline (about 0 V at ADC = 2,050 ch), but undershoot was observed in our experiments (see Methods section 'Initial flash'). An energy of 10 MeV corresponds to ADC increases of 1,395 ch, 1,218 ch and 404 ch for detectors A, B and C, respectively. The data gap for detector A is due to overflow of memory buffer in the ADC board.

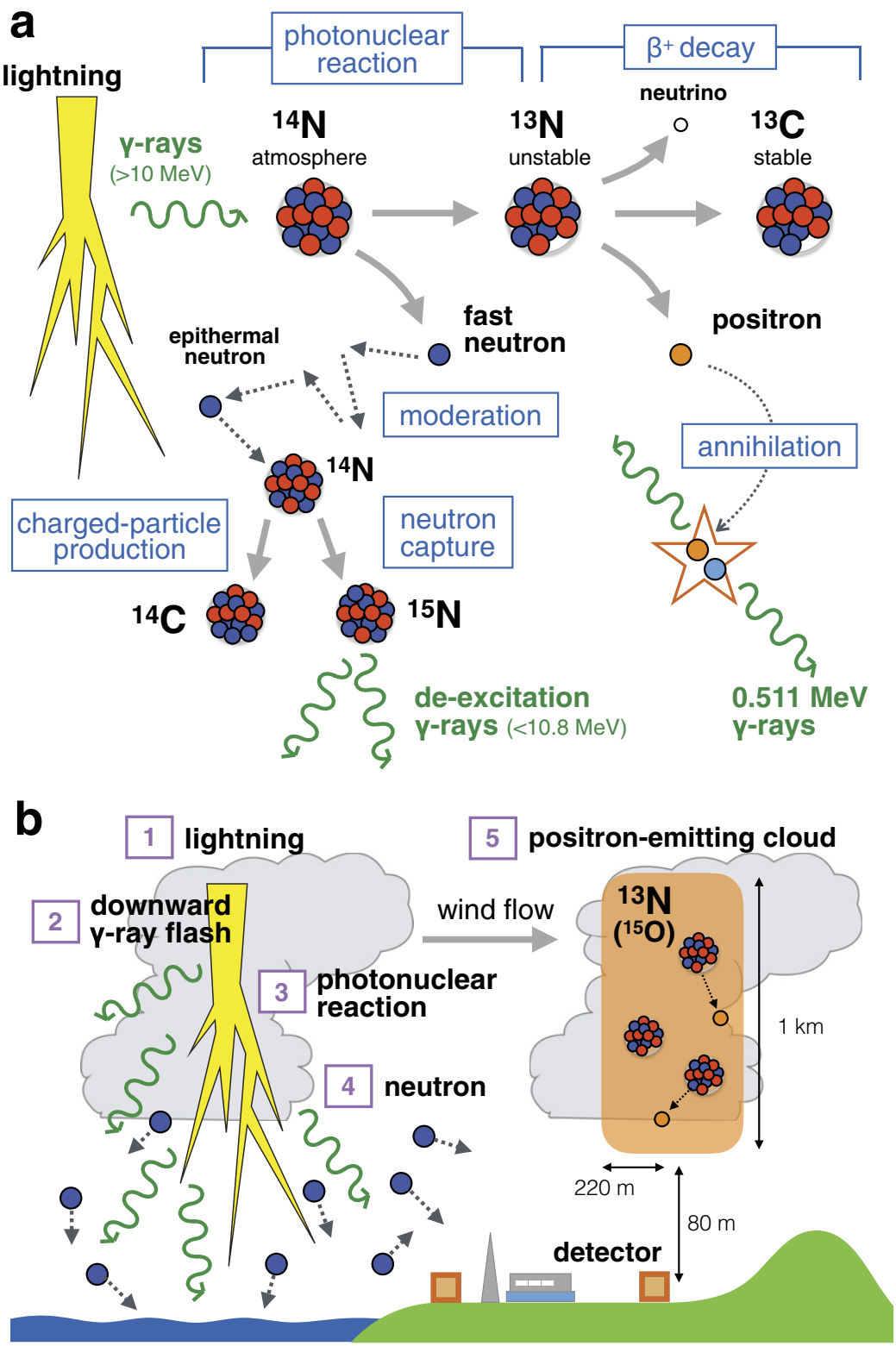

Extended Data Figure 3 | Illustration of lightning-triggered physical processes. a, Physical processes during a chain of radiation events induced by the photonuclear reactions. **b**, Diffusion of neutrons produced in lightning and drift of the positron-emitting cloud.

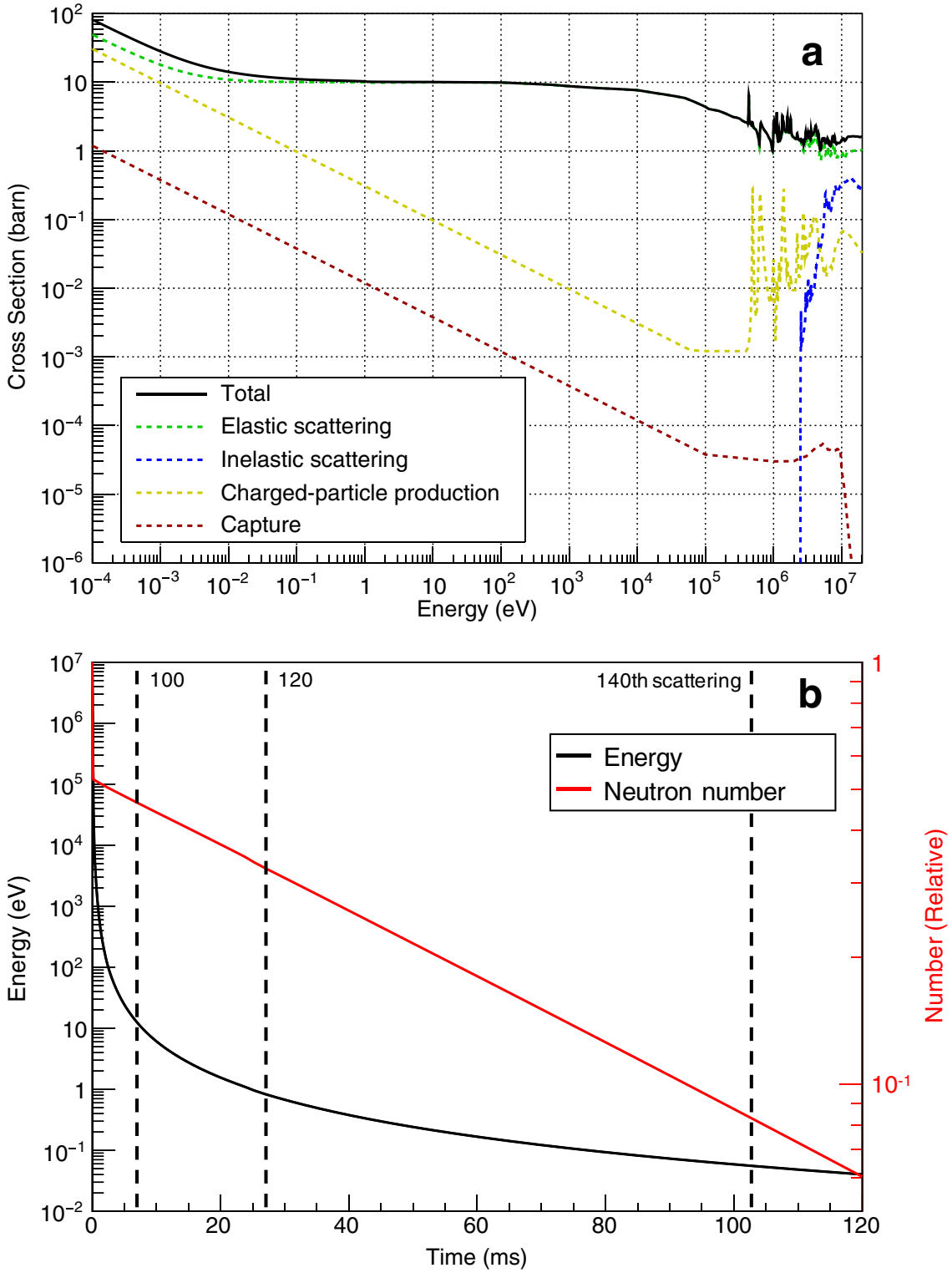

Extended Data Figure 4 | Neutron cross-section on nitrogen and time profile of scattered neutrons. a, Neutron cross-section on ^{14}N (black) as a function of neutron kinetic energy[40,41], including elastic (green) and inelastic (blue) scattering, charged-particle production (yellow) and neutron capture (red). **b**, Kinetic energy (black) and relative number of neutrons (red) as a function of time. The initial energy of neutrons is assumed to be 10 MeV and the initial number of neutrons is normalized to 1. Dashed lines indicate the times of the *n*th scatterings.

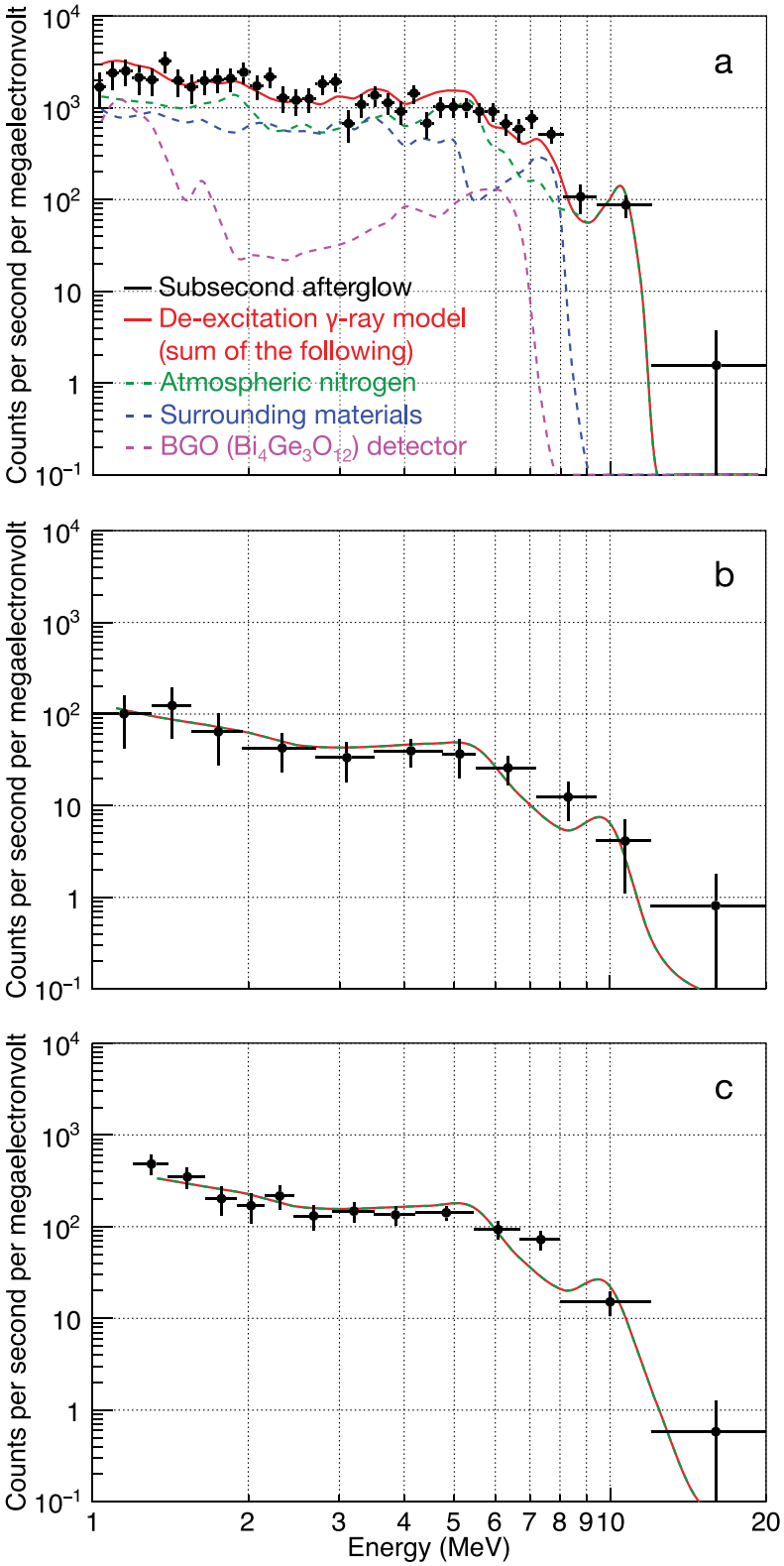

Extended Data Figure 5 | De-excitation γ-ray spectra compared with simulations. a–c, Background-subtracted γ-ray spectra of the subsecond γ-ray afterglow, with black crosses indicating $\pm 1\sigma$ errors, for detectors A (**a**), B (**b**) and C (**c**). The source events are extracted for the period $t = 40$–100 ms for detector A and $t = 20$–200 ms for detectors B and C. The curves show the Monte Carlo simulations of de-excitation γ-rays from atmospheric nitrogen (green dashed line), surrounding materials (blue dashed line), the detector itself (magenta dashed line) and their total (red solid line). The simulated spectra are normalized by the total counts above 1 MeV.

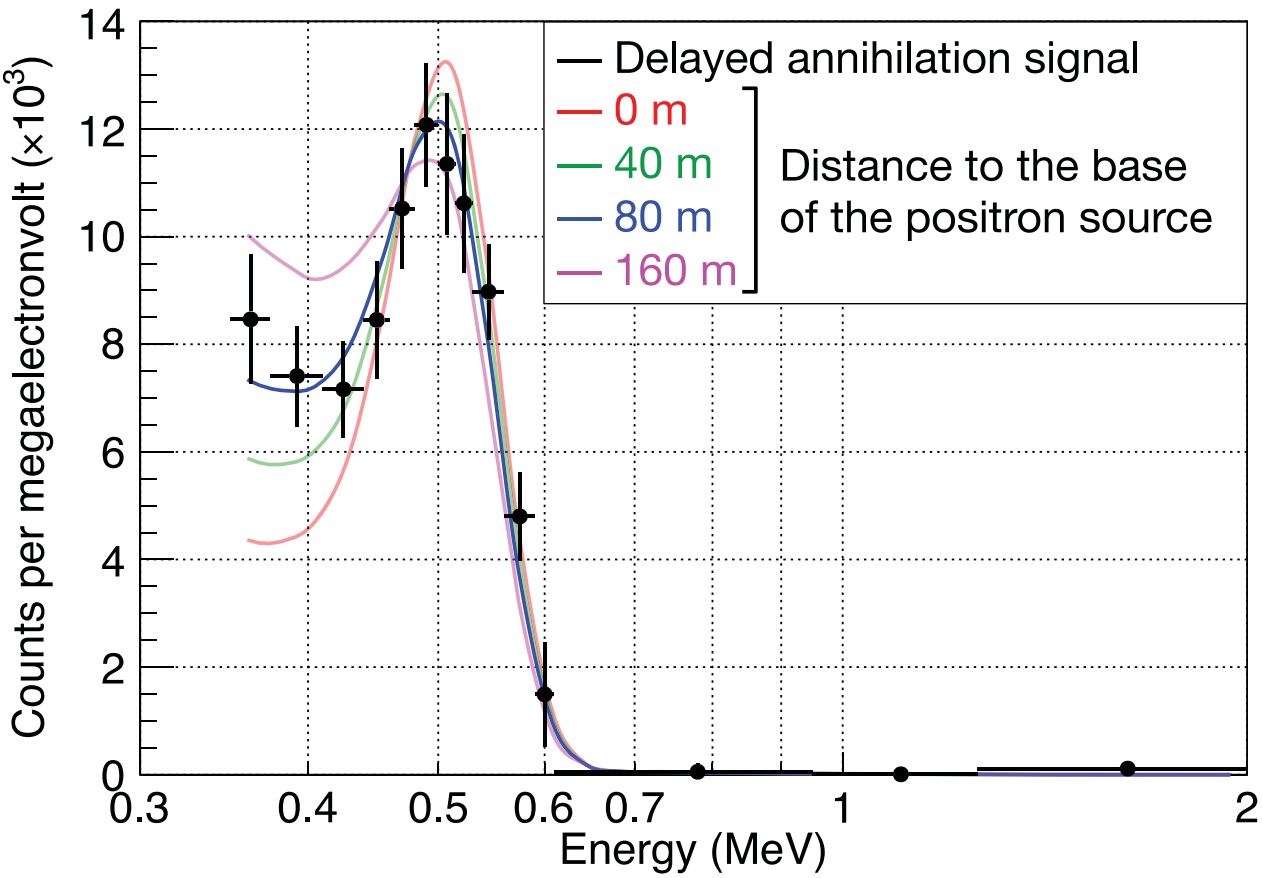

Extended Data Figure 6 | Observed annihilation spectrum and simulated models. The background-subtracted spectrum in the delayed phase for detector A, accumulated over $t = 11.1–62.8$ s, is plotted, with black crosses indicating $\pm 1\sigma$ errors. The simulated model curves are overlaid, for assumed distances to the base of the positron-emitting cloud of 0 m (that is, the detector is within the cloud; red), 40 m (green), 80 m (blue) and 160 m (magenta). The models are normalized by the total counts in the 0.4–0.6-MeV band.

Extended Data Table 1 | Specifications of our detectors and values obtained

Detector	A	B	C	D
Longitude	138.5960° E	138.6058° E	138.6014° E	138.5907° E
Latitude	37.4211° N	37.4222° N	37.4267° N	37.4200° N
Scintillation crystal	Cuboid BGO	Cuboid BGO	Cuboid BGO	Cylindrical NaI
Size (cm)	25 × 8 × 2.5	25 × 8 × 2.5	25 × 8 × 2.5	7.62 × ϕ7.62
PMT type	2 × R1924A	2 × R1924A	2 × R1924A	R6231
Energy range (MeV)	0.35–13.0	0.35–13.0	1.2–48.0	0.2–27.0
Energy resolution (MeV) at 0.511 MeV	0.109 ± 0.002	0.090 ± 0.001	out of range	0.055 ± 0.001
		Initial radiation flash		
Undershoot dead time (ms)	< 40	< 20	< 20	< 300
		Sub-second afterglow		
Decay constant	56 ± 3	55 ± 12	36 ± 4	undershoot
Detected counts (20–200 ms)	1530	132	177	863
Energy range (MeV)	> 0.35	> 0.35	> 1.20	> 0.20
		Prolonged annihilation signal (0.511 MeV line)		
Photon counts	1830 ± 240	< 30 (1σ)	out of range	366 ± 50
(Delayed component)	(1360 ± 210)	–	–	–
Line centre (MeV)	0.515 ± 0.008	–	–	0.501 ± 0.007
Line FWHM	0.120 ± 0.009	–	–	0.061 ± 0.007
Effective area (cm^2) at 0.511 MeV	149.2	149.2	out of range	28.3

Errors are $\pm 1\sigma$.